Earth and Planetary Science Letters 409 (2015) 290–298

Contents lists available at ScienceDirect

Earth and Planetary Science Letters

www.elsevier.com/locate/epsl

No late Quaternary strike-slip motion along the northern Karakoram fault

Alexander C. Robinson [a,*], Lewis A. Owen [b], Jie Chen [c], Lindsay M. Schoenbohm [d], Kathryn A. Hedrick [b], Kimberly Blisniuk [e], Warren D. Sharp [e], Daniel B. Imrecke [a], Wenqiao Li [c], Zhaode Yuan [c], Marc W. Caffee [f,g], Regina Mertz-Kraus [e,1]

[a] Department of Earth and Atmospheric Sciences, University of Houston, Houston, TX 77204, USA
[b] Department of Geology, University of Cincinnati, Cincinnati, OH 45221, USA
[c] State Key Laboratory of Earthquake Dynamics, Institute of Geology, China Earthquake Administration, Beijing 100029, China
[d] Department of Earth Sciences, University of Toronto, Toronto, Ontario, M5S 3B1, Canada
[e] Berkeley Geochronology Center, 2455 Ridge Rd., Berkeley, CA 94709, USA
[f] Department of Physics/PRIME Laboratory, Purdue University, West Lafayette, IN 47906, USA
[g] Department of Earth, Atmospheric, and Planetary Sciences, Purdue University, West Lafayette, IN 47906, USA

ARTICLE INFO

Article history:
Received 24 July 2014
Received in revised form 4 November 2014
Accepted 7 November 2014
Available online xxxx
Editor: A. Yin

Keywords:
Karakoram fault
Quaternary
fault evolution
Tibet
strike-slip
neotectonics

ABSTRACT

Models that treat long-term evolution of the Tibetan orogen in terms of interactions between rigid blocks require the right-slip Karakoram fault that bounds the western margin of the Tibetan plateau to be a long-lived, stable, high slip-rate feature. While the southern portion of the fault clearly remains active, recent work has proposed that the northern half of the Karakoram fault is currently inactive. New field observations and geochronologic results from the northern end of the Karakoram fault system confirm this interpretation and provide the first quantitative data on the minimum age for the termination of slip. In the southeast Pamir, gravel that yields a U-series age of 198 ± 5 ka on secondary carbonate caps a non-deformed strath terrace that extends across the main strand of the Karakoram fault. The secondary Achiehkopai fault strand is overlain by undisturbed Hangdi glacial stage (24 ± 6 ka) deposits and Dabudar glacial stage (penultimate glacial cycle, ~150 ka, or older) deposits, which lack observable lateral displacement or deformation. Together, these observations show that the northern portion of the Karakoram fault system has not accommodated any detectable strike-slip deformation since at least 24 ± 6 ka, and most likely since ~200 ka or more. These results show that the Karakoram fault system no longer forms a continuous discrete kinematic boundary at the western margin of the Tibetan Plateau. This suggests that even long (>500 km) strike-slip faults within orogenic belts are inherently unstable features, consistent with models of continental collision zones involving relatively weak crust and distributed deformation.

1. Introduction

A critical aspect of understanding the tectonic evolution of orogenic belts is determining the extent to which deformation of continental crust is best modeled as a continuum with distributed deformation, or as rigid plates with discrete boundaries. This discussion has been particularly persistent in the Himalayan–Tibetan orogen, where ongoing debate has focused on the role and prominence of regional scale strike-slip faults such as the Altyn Tagh, Kunlun, Red River, and Karakoram faults, as well as numerous smaller faults (Molnar and Tapponnier, 1978; Replumaz and Tapponnier, 2003; Tapponnier et al., 1982; Thatcher, 2007). While numerical models can simulate the observed geodetic velocity fields with various distributions of quasi-rigid microplates (Loveless and Meade, 2011; Meade, 2007; Thatcher, 2007), a critical question for understanding the viability of plate-like models over geologic timescales (generally on the order of 10^5–10^7 years) is the stability of block bounding faults.

A key structure in all Tibetan plate-like models is the ~1200 km long right-slip Karakoram fault, which is required to be long-lived (~25 Ma), stable fault accommodating a high slip rate (~10 mm/yr) along its entire trace from the Pamir to the Himalaya (Avouac and Tapponnier, 1993; Chevalier et al., 2011, 2012;

* Corresponding author.
E-mail address: acrobinson@uh.edu (A.C. Robinson).
[1] Present address: Institute for Geosciences, Johannes Gutenberg University, Mainz, Germany.

http://dx.doi.org/10.1016/j.epsl.2014.11.011
0012-821X/

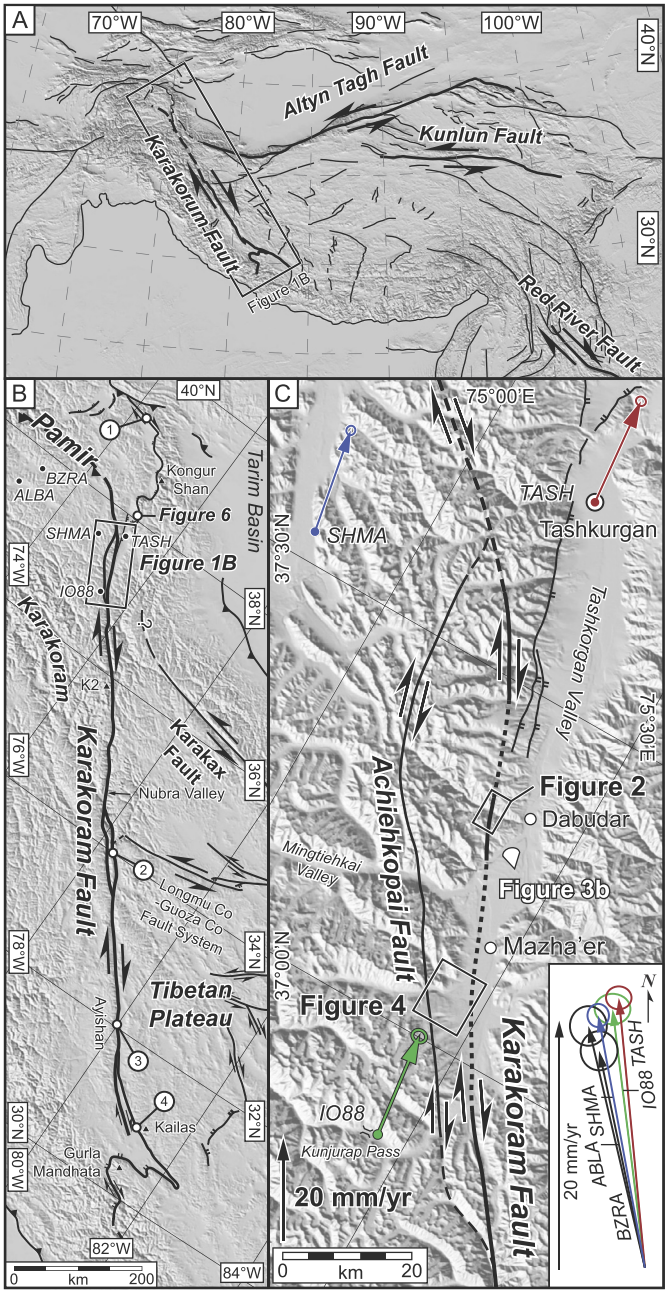

Fig. 1. A) Simplified regional map of the Himalayan–Tibetan orogen showing active faults modified from Taylor and Yin (2009). B) Map of the Karakoram fault system showing the trace of the Karakoram and related faults, and documented active structures in western Tibet, and locations of several GPS stations in the Southern Pamir (from Ischuk et al., 2013; Zhang et al., 2004). Numbered locations denote previous studies cited in text: (1) Chevalier et al. (2011); (2) Brown et al. (2002); (3) Chevalier et al. (2005); (4) Chevalier et al. (2012). C) Map of the southeast Pamir showing faults of the Karakoram fault system and the active Kongur Shan extensional system. GPS velocity vectors are relative to stable Eurasia (Ischuk et al., 2013; Zhang et al., 2004). Boxes show locations of Figs. 2 and 4. Inset shows a direct comparison of the GPS velocity vectors from stations in B. (For interpretation of the references to color in this figure legend, the reader is referred to the web version of this article.)

He and Chéry, 2008; Liu and Bird, 2008; Loveless and Meade, 2011; Meade, 2007; Peltzer and Saucier, 1996; Thatcher, 2007; Valli et al., 2007) (Fig. 1A and B). If so, it would strongly support the interpretation that the Karakoram fault is lithospheric in scale, and would have important implications for strain localization and the rheological behavior of orogen interiors. In addition to its role as a regional block-bounding structure, this model carries the important implication that deformation in the Pamir–Karakoram region at the western end of the Himalayan–Tibetan orogen is partially decoupled from that of the Tibetan Plateau. Alternatively, studies that find lower displacement and slow slip rates on the Karakoram fault suggest a more complex and limited role in the orogen. Resolving these different interpretations is important for understanding how strain related to the India–Asia collision has been accommodated at the western end of the Himalayan–Tibetan orogen, and the mechanical behavior of continental crust.

While the southern half of the Karakoram fault clearly accommodates active slip (Armijo et al., 1989; Brown et al., 2002; Chevalier et al., 2005, 2012; Murphy et al., 2014) the Quaternary slip history of the northern half of the fault is debated. Recent work based on interpretation of satellite images suggests that the northern end of the Karakoram fault (where it enters the Pamir) has not been active since at least the late Quaternary (Robinson, 2009a), while a study along the Muji segment of the Kongur Shan extensional system to the north suggests the entire Karakoram fault is active with a slip rate of ~10 mm/yr (Chevalier et al., 2011). Here we report direct field observations coupled with new and previously published geochronologic results along the southern Tashkorgan valley that show the northern portion of the Karakoram fault has not accommodated any detectable slip in the late Quaternary.

2. Geologic setting

2.1. Regional geology

The ~1200 km right-slip Karakoram fault defines the western margin of the Tibetan orogen, separating the Pamir–Karakoram Mountains to the west from the Tibetan Plateau to the east (Fig. 1A and B). The role and relative importance of the Karakoram fault has been a topic of considerable debate over several decades, with interpretations ranging from the fault accommodating hundreds of km of slip and playing a central role in the evolution of the Himalayan–Tibetan orogen (e.g. Avouac and Tapponnier, 1993; Lacassin et al., 2004; Peltzer and Tapponnier, 1988; Tapponnier et al., 1982), to interpretations of more modest amounts of slip with the fault playing a limited role in the orogen (Murphy et al., 2000; Phillips et al., 2004; Robinson, 2009b; Searle, 1996; Searle et al., 2011, 1998).

Documented displacements along the Karakoram fault generally favor the latter of these models, as do significant along-strike variations in the amount of offset. The northern portion of the fault system has accommodated ~150 km of displacement (Robinson, 2009b), decreasing to ~65 km of displacement along the southern portion of the Karakoram fault (Murphy et al., 2000; Wang et al., 2012). While this along strike variation suggests a complex, and possibly evolving role within the Himalayan–Tibetan orogen, the current role and importance of the Karakoram fault in accommodating strain related to the India–Asia collision is still not well resolved. Several studies of offset geomorphic features have proposed relatively rapid Quaternary slip rates on the Karakoram fault of 7–12 mm/yr along the entire trace of the fault from southeast Tibet to the Pamir (Fig. 1B) (Chevalier et al., 2011, 2005, 2012). Other studies yield considerably slower Quaternary slip rates along the southern portion of the fault system (~4 mm/yr; Brown et al., 2002, 2005), or have suggested that the northern portion of the Karakoram fault has been inactive during the Quaternary (Robinson, 2009a) with active extension along the Kongur Shan extensional system unrelated to slip on the Karakoram fault (Robinson et al., 2004, 2007). Regional geodetic studies also give variable results with GPS studies along the southern portion of the fault yielding slip rates of 5 ± 2 mm/yr (Kundu et al., 2014), to 11 ± 4 mm/yr (Banerjee and Burgmann, 2002), and regional InSAR results yielding slip rates that vary along

strike from 0 mm/yr to ~5 mm/yr (Wang and Wright, 2012; Wright et al., 2004). These variable results highlight the importance of better documenting the Quaternary slip history of the Karakoram fault to understand its role in the India–Asia collision zone.

2.2. Local geologic setting and Quaternary deposits

The northern Karakoram fault system, defined by truncated bedrock units, crosses the southern end of the Tashkorgan valley in the southeast Pamir of western China. Here, the fault splits into two strands; the main strand of the Karakoram fault to the east, and a secondary strand to the west, the Achiehkopai fault (Robinson, 2009b) (Fig. 1C). Previous interpretation of satellite images found no evidence of other possible fault strands in the area, either active or inactive, that could be related to the Karakoram fault (Robinson, 2009b). This is supported by our field observations from numerous traverses along east–west trending valleys on the eastern side of the Tashkorgan valley, as well as further analysis of detailed satellite images available through Google Earth along the ~65 km long east–west trending Mingtiehkai river valley to the west.

Along the southern end of the Tashkorgan valley, both identified fault strands are overlain by a series of Quaternary glacial and glaciogenic landforms and sediments. This area is one of the only locations along the northern portion of the Karakoram fault where multiple generations of Quaternary deposits directly overly the trace of the Karakoram fault strands. Morphostratigraphic analysis and cosmogenic ^{10}Be surface exposure dating of these landforms and deposits define four main glacial stages in the Tashkorgan valley (Owen et al., 2012): 1) the Dabudar glacial stage interpreted to be older than or equivalent to the penultimate glacial cycle (~150 ka); 2) the Tashkorgan glacial stage that dates to 66 ± 10 ka (^{10}Be uncertainties given as 1σ); 3) the Hangdi glacial stage that dates to 24 ± 6 ka; and 4) the Kuzigan glacial stage that dates to 16 ± 6 ka. In this study we focus on two sites in the region with well-defined geomorphic markers from the oldest identified glacial stages that lie directly along the strands of the Karakoram fault. Our observations, integrated with new geochronologic data and our previously published ^{10}Be surface exposure ages, show the northern Karakoram fault in the Tashkorgan Valley has not accommodated any detectable slip during the latter part of the Quaternary.

3. Field observations

3.1. Pisiling site

West of the town of Dabudar in the southern Tashkorgan valley, the main strand of the Karakoram fault trends orthogonally across a narrow bedrock valley at the village of Pisiling (Figs. 1C, 2, and Supplementary Fig. DR1). Here, a well-developed strath terrace which lies ~50 m above the active drainage extends across the ~100 m wide Karakoram fault zone (Fig. 3A and Supplementary Fig. DR2A). This strath terrace is overlain by ~10 m of coarse fluvial gravels and sands with a discontinuous 1–2 m thick calcite cemented zone at their base, which are in turn overlain by colluvium. Our field observations document two key aspects of the landforms in the valley: 1) neither the fluvial strath nor the overlying terrace deposits show any sign of tectonic disturbance (e.g. brecciation or disruption of bedding) where they overly the Karakoram fault; and 2) the riser of the strath terrace shows no lateral separation across the trace of the Karakoram fault (Fig. 2). Consistent with previous interpretations of satellite images (Robinson, 2009a; Robinson et al., 2007), other landforms in the area that cross the fault zone show no lateral separation or tectonic disturbance, including numerous small drainages orthogonal to the fault zone and topographic ridges capped by Dabudar stage glacial deposits (Fig. 2).

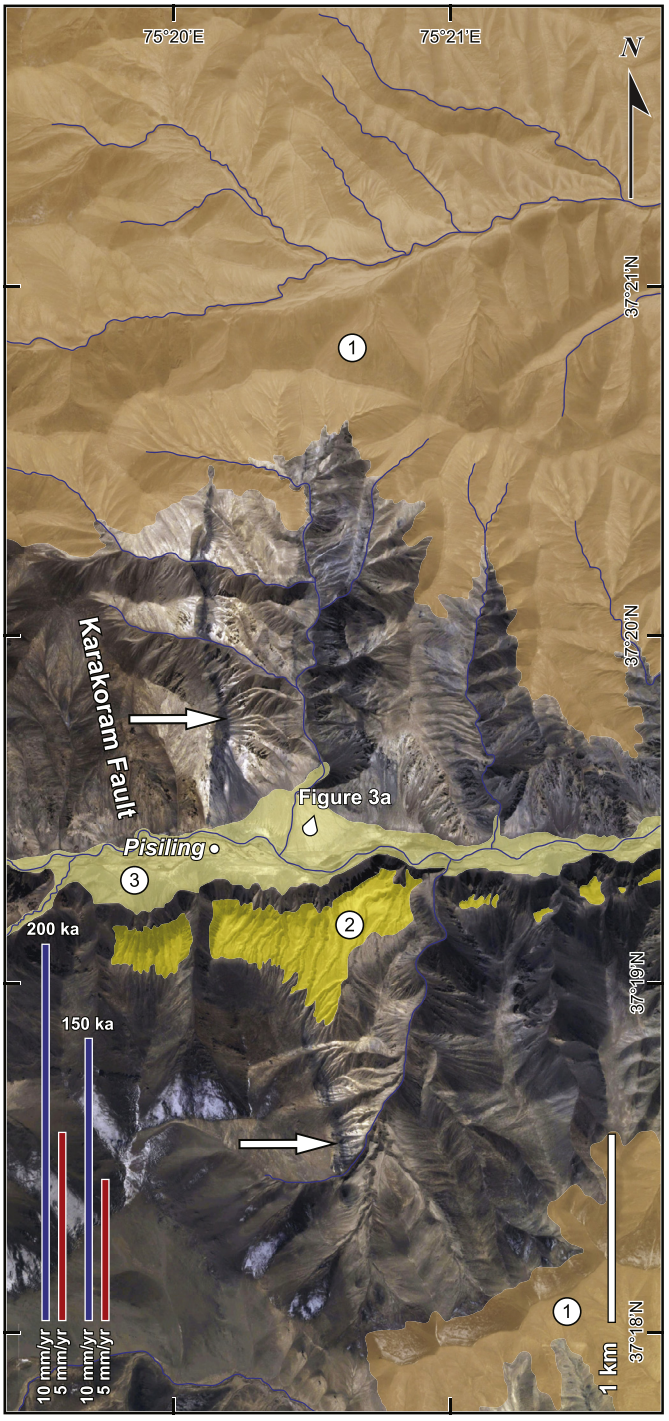

Fig. 2. Annotated satellite image of the Pisiling field site showing the Karakoram fault damage zone defined by the white and black rocks (white arrows), drainages (blue lines), and surficial deposits: (1) Dabudar glacial stage deposits; (2) Fluvial deposits overlying a strath terrace; and (3) Recent stream deposits. Bars in lower left show expected displacements of 150 ka, and 200 ka landforms for slip rates of 5 mm/yr (red) and 10 mm/yr (blue).

3.2. Dabudar site

Immediately southeast of the Pisiling field site described above, a well-developed terrace ~50 m above the valley floor is exposed

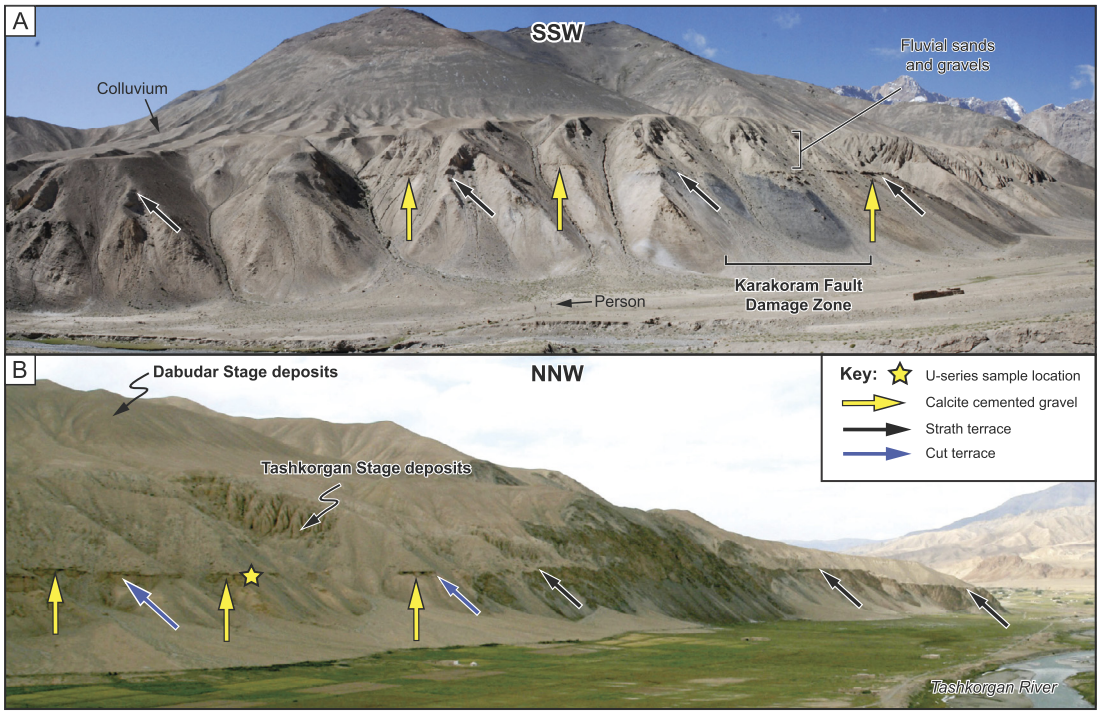

Fig. 3. A) Strath terrace (black arrows) at the Pisiling site developed directly on the Karakoram fault zone. The strath terrace is capped by discontinuous calcite cemented gravel (yellow arrows). B) Strath terrace (black arrows) and cut terrace (blue arrows) at the Dabudar site. The terrace is capped by a discontinuous calcite cemented gravel, and overlain by Tashkorgan stage glacial deposits (Owen et al., 2012). Dabudar Stage deposits are exposed at higher elevations in the background. Star shows location of sampled calcite cemented gravel used in U-series geochronology. (For interpretation of the references to color in this figure legend, the reader is referred to the web version of this article.)

along the western side of the main Tashkorgan valley (Figs. 3B, Supplementary Figs. DR2B, DR3). The terrace occurs both as a strath terrace developed on Paleozoic bedrock and as a cut terrace developed on earlier Quaternary deposits (Owen et al., 2012). As at the Pisiling site, a discontinuous layer of calcite cemented gravel up to ~2 m thick forms the basal part of overlying glaciofluvial deposits (Owen et al., 2012). We interpret the terraces and the cemented conglomerate layers at the two sites to be isochronous based on their similar elevations above the active drainages, field observations and satellite images which show a series of terrace remnants at similar elevations that can be traced continuously between the two sites (Supplementary Fig. DR3), and the identical appearance of the calcite-cemented gravels in both locations.

3.3. Mazha'er site

South of the town of Mazha'er, ~30 km south of the sites described above, both strands of the Karakoram fault are overlain by several generations of glacial and glaciofluvial deposits (Figs. 1C, 4, and Supplementary Fig. DR4). Within the center of the Tashkorgan valley the projection of the main strand of the Karakoram fault is overlain by hummocky Tashkorgan glacial stage moraines and deposits (Owen et al., 2012; Robinson, 2009a). Field observations and interpretation of high-resolution satellite images available on Google Earth confirm the previous interpretation that these deposits have not experienced any tectonic disturbance or lateral offset (Robinson, 2009a).

Immediately to the southwest along the margin of the valley, the trace of the Achiehkopai strand is overlain by Dabudar glacial stage deposits (~150 ka or older), and a Hangdi glacial stage moraine (mean ^{10}Be age of 24 ± 6 ka, uncertainty = 1σ) (Owen et al., 2012). The Hangdi glacial stage deposits in this location show no lateral displacement or tectonic disturbance. In contrast, the Dabudar stage deposits have distinct NW trending

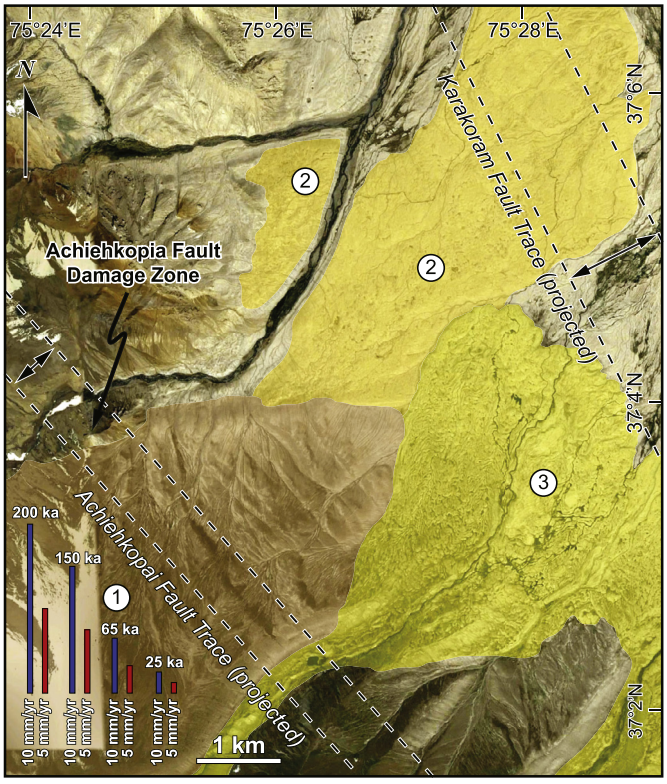

Fig. 4. Annotated satellite image of the Karakoram fault system near Mazha'er showing the projected trace of the Achiehkopai and Karakoram faults and different glacial stage surficial deposits (Owen et al., 2012): (1) Dabudar Stage; (2) Tashkorgan Stage; and (3) Hangdi Stage. Bars in lower left show expected displacements of 25 ka, 65 ka, 150 ka, and 200 ka landforms for slip rates of 5 mm/yr (red) and 10 mm/yr (blue).

topographic scarps that are sub-parallel to the Achiehkopai strand (Owen et al., 2012; Robinson, 2009a). Field observations and high-resolution satellite images document several critical features of the scarps (Fig. 4): 1) small stream drainages that cross the scarps show no observable lateral separation; 2) where Dabudar glacial stage deposits are deposited directly against the bedrock fault zone along their northern margin there is no lateral separation of the contact; 3) the largest, westernmost scarp is concave towards the valley, with the smaller, closely spaced, more linear scarps appearing to terminate into it; and 4) the scarps in the Dabudar glacial stage moraine are highly degraded and do not continue into the Tashkorgan or Hangdi glacial stage moraines, showing they developed prior to ~65 ka. Further, the lack of identifiable faults in the bedrock directly along-strike to the NW supports the previous interpretation that these features are not tectonic in nature and are not related to strike-slip deformation along the northern Karakoram fault zone. Rather, these features most likely reflect basinward slumping of the deposits prior to the Tashkorgan glacial stage, with the toe of the slump removed during subsequent deposition and erosion.

4. U-series geochronology

To limit the age of the terraces at the Pisiling and Dabudar sites described above, we performed U-series dating of secondary carbonate clast-coatings from the gravel unit capping the strath at the Dabudar site to obtain a minimum depositional age (Fig. 3B and Supplementary Fig. DR5). While several samples were collected from the site, only one sample yielded clean enough clast coatings for dating. The dated carbonate consists of off-white radiaxial coatings typically two to three millimeters thick, which completely enclose the gravel-clasts (Supplementary Fig. DR5). While such coatings are known to form by pedogenesis, we consider it most likely that the dated coatings formed from groundwater deposition. This interpretation follows from the observations that: (1) the conglomerate is located at the base of ~10 m of rapidly deposited fluvial sediments that otherwise lack evidence of calcic pedogenesis; (2) unlike pedogenic coatings that are thicker on the bottoms of clasts, those on the pebbles from the Dabudar gravels are of uniform thickness; and (3) the conglomerate occurs at the interface between highly permeable sediments above and less permeable bedrock and older sediments below, making it a likely pathway for lateral groundwater flow. We note, however, that our interpretation of the U-series age of the coatings as a minimum depositional age for the host gravel is independent of the mode of origin of the coatings.

4.1. Sample preparation

Our initial analyses ("whole coatings" in Table 1) were performed on samples from seven different clasts (a and c–h). These samples included essentially the entire thickness of each coating and were cleaned ultrasonically to remove detritus and clay films. The resulting ages are imprecise due to high levels of common Th (^{232}Th) and show considerable scatter (see Results below).

In light of the first round of analyses, we carried out additional analyses using a modified sample preparation procedure, as follows. Inner coatings were prepared by: (1) abrading the outer surfaces of the selected coatings with a diamond dental burr to remove outer (and presumably younger) layers of carbonate; (2) separating coatings from their host clasts with a tool steel knife blade; (3) lightly abrading their inner surface to remove ^{232}Th-rich clay films; (4) cleaning in an ultrasonic bath; and (5) breaking the abraded inner coating from each clast into sub-samples designated "1" and "2". We analyzed two sub-samples each from three pebbles (a–c) for a total of six ages obtained using this protocol ("abraded

Table 1
U–Th isotopic data and ages of secondary carbonate clast-coatings from gravels at the Dabudar study site. Sample location: 37.30208°N; 75.39519°E.

Sample name	Sample wt. (mg)	U (ppb)	^{232}Th (ppb)	(^{230}Th/^{232}Th)	(^{232}Th/^{238}U)	± (%)	(^{230}Th/^{238}U)	± (%)	(^{234}U/^{238}U)	± (%)	Uncorrected age, error (ka)	Corrected age, error (ka)	Initial (^{234}U/^{238}U), ± (abs.)	
Abraded inner coatings														
UK1-a1	2.60	449.6	333.3	4.171	0.24099	0.21	1.0052	0.38	1.1402	0.32	211.1	192	±16	1.301 ±0.048
UK1-a2	3.02	470.0	144.4	9.404	0.10010	0.16	0.94135	0.53	1.1370	0.27	179.3	171.7	±6.1	1.242 ±0.017
UK1-b1	8.76	450.9	160.7	8.635	0.11605	0.13	1.0021	0.43	1.1224	0.26	221.4	212.5	±9.0	1.247 ±0.020
UK1-b2	9.26	455.8	330.0	4.085	0.23531	0.14	0.96117	0.33	1.1215	0.12	197.1	178	±15	1.249 ±0.043
UK1-c1	6.68	399.0	134.5	8.964	0.10950	0.13	0.98158	0.29	1.1338	0.31	201.3	193.0	±7.2	1.254 ±0.019
UK1-c2	5.31	411.4	257.7	4.986	0.20393	0.12	1.0168	0.29	1.1352	0.19	221.9	206	±15	1.291 ±0.039
Whole coatings														
U1-a	9.95	937.0	875.6	1.354	0.30383	0.34	0.41136	0.22	1.1605	0.213	47.26	±0.09	21.0	±12 1.227 ±0.023
U1-c	9.47	575.6	540.5	2.203	0.30552	0.30	0.6729	1.2	1.1428	0.257	94.68	±0.9	68.4	±12 1.232 ±0.026
U1-d	9.37	482.4	922.7	1.509	0.62358	0.18	0.9411	1.4	1.1399	0.583	178.1	±3.3	117.6	±40 1.402 ±0.111
U1-e	9.96	430.2	752.2	1.713	0.56880	0.29	0.97426	0.21	1.1295	0.514	199.9	±1.8	146.2	±44 1.369 ±0.090
U1-f	9.21	719.8	385.6	3.154	0.17471	0.30	0.55110	0.23	1.1644	0.335	68.75	±0.20	54.7	±6.1 1.224 ±0.013
U1-g	8.82	574.4	3023	0.467	1.7200	0.28	0.80336	0.26	1.0963	0.376	139.6	±0.7	nr	nr
U1-h	10.03	441.9	1645	0.713	1.2119	0.30	0.86444	0.16	1.113	1.561	156.5	±3.1	nr	nr

All isotope ratios are activity ratios. Uncertainties are given at 1 standard deviation. Uncorrected ages are calculated without correction for U and Th from detritus. Corrected ages are calculated assuming detritus with (^{232}Th/^{238}U) = 1.2 ± 0.6, (^{230}Th/^{238}U) = 1.0 ± 0.1, and (^{234}U/^{238}U) = 1.0 ± 0.1. (^{234}U/^{238}U) initial is back-calculated from measured ratio and corrected age. Decay constants are those of Jaffey et al. (1971) for ^{238}U and Cheng et al. (2013) for ^{230}Th and ^{234}U. "nr" indicates corrected age and initial U ratio not reported due very large detritus correction. See text on U-series sample preparation for explanation of "whole coatings" and "abraded inner coatings".

inner coatings" in Table 1). Compared to ages from the whole coatings, those from the abraded samples are more precise, less dispersed, and older, as expected (Table DR1).

4.2. U-series methods

Analyses were performed at the Berkeley Geochronology Center using a Thermo Neptune *Plus* Multi-Collector-Inductively-Coupled-Mass-Spectrometer (MC-ICP-MS). Samples were totally dissolved in 7 N HNO_3 and equilibrated with a mixed spike containing ^{229}Th, ^{233}U, and ^{236}U. The spike was calibrated using solutions of NBL CRM 145 and solutions prepared from a 69 Ma U ore that has been demonstrated to yield concordant U–Pb ages (Schwartzwalder Mine, Colorado, USA; hereafter, SM) and sample-to-sample agreement of ^{234}U/^{238}U and ^{230}Th/^{238}U ratios. U and Th were separated using two stages of HNO_3–HCl cation exchange chemistry followed by reaction with HNO_3 and $HClO_4$ to remove any residual organic material. Measured peak heights were corrected for peak tailing, multiplier dark noise/Faraday baselines, instrumental backgrounds, ion counter yields, mass fractionation, interfering spike isotopes, and procedural blanks. Mass fractionation was determined using the gravimetrically determined ^{233}U/^{236}U ratio of the spike. The external reproducibility of ^{234}U/^{238}U and ^{230}Th/^{238}U ratios of SM solutions measured during each run was better than 0.2%. Ages were calculated using the half-lives of Jaffey et al. (1971) for ^{238}U, Holden (1989) for ^{232}Th, and Cheng et al. (2013) for ^{230}Th and ^{234}U. Correction for U and Th from detritus was made assuming detritus with activity ratios of $(^{232}\text{Th}/^{238}\text{U}) = 1.2 \pm 0.6$, $(^{230}\text{Th}/^{238}\text{U}) = 1.0 \pm 0.1$, and $(^{234}\text{U}/^{238}\text{U}) = 1.0 \pm 0.1$, which correspond to average silicate crust in secular equilibrium. Ages and uncertainties were calculated with Isoplot (Ludwig, 2003). Uncertainties of corrected ages include measurement errors and uncertainties associated with the detritus correction.

4.3. Results

We obtained seven ages on the samples from the whole coatings, which ranged in age from 21 ± 12 to 146 ± 44 ka. As mentioned above, the large error and scatter of the data indicate significant common Th (^{232}Th) contamination, and as such the ages do not reliably record the age of the calcite coatings. The results from our initial round of analyses are not discussed further.

We obtained six ages on the samples from abraded inner coatings that range from 172 ± 6 to 213 ± 9 ka (1σ; Fig. 5). The five oldest ages obtained for the abraded samples are in good agreement (MSWD = 1.3, probability of fit = 0.26) and have a weighted mean age of 198 ± 5 ka (uncertainty given as 1σ). We interpret this age as a robust minimum estimate of the depositional age of the host terrace gravels at the Dabudar site, and by correlation a minimum estimate of the depositional age of the terrace gravels at the Pisiling site.

5. Discussion

5.1. Late Quaternary slip history of the northern Karakoram fault

Field observations presented here, coupled with our new and previously published geochronology, allow us to assess the late Quaternary slip history of the northern Karakoram fault. At the Pisiling site, our U-series ages from gravels overlying a correlative strath from the Dabudar site indicate a minimum age of 198 ± 5 ka for the undisturbed strath terrace developed directly across the main strand of the Karakoram fault, providing a robust minimum for the age of termination of slip on this strand. Additionally, field relations which indicate that development of the strath terrace post-dates Dabudar glacial stage deposits provide further evidence

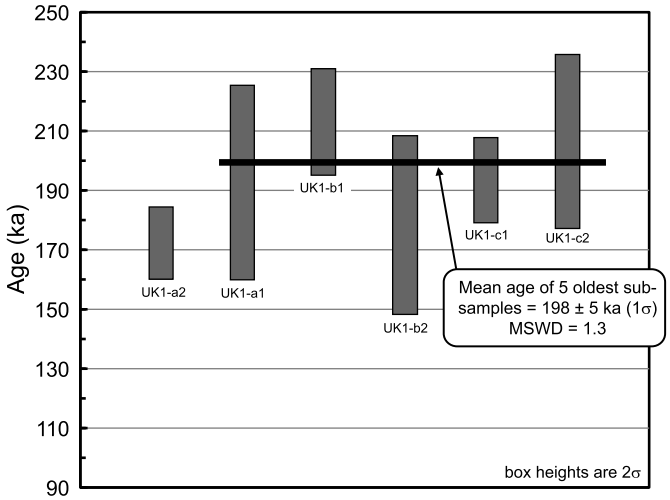

Fig. 5. Plot of U-series ages for abraded inner clast-coatings from gravel at the Dabudar site.

that the deposits pre-date the penultimate glacial cycle and are older than 200 ka (Owen et al., 2012). The undisturbed nature of the Dabudar glacial stage deposits overlying the main strand of the Karakoram fault strengthens our interpreted minimum age of termination.

Along the Achiehkopai fault strand, the undisturbed nature of the Hangdi glacial stage deposits directly overlying the strand similarly provide a robust minimum age of 24 ± 6 ka for termination of slip. Additionally, the Dabudar glacial stage deposits that show no lateral separation where they overlie the Achiehkopai fault strand indicate that neither strand of the northern Karakoram fault has carried detectable slip for ~200 ka or longer. While this interpretation is not as robust as for the Hangdi glacial stage deposits given the highly eroded nature of the Dabudar glacial deposits, Dabudar glacial stage landforms would be expected to show 1–2 km of lateral offset for slip rates of 5–10 mm/yr (Chevalier et al., 2011, 2005), which they clearly do not. Further, the truncation of the topographic scarps in the Dabudar glacial stage deposits by the Tashkorgan glacial stage deposits show they are older than 65 ka, regardless of their origin.

Together, our observations from the Pisiling and Mazha'er sites show that the northern end of the Karakoram fault system has not accommodated any detectable strike-slip deformation since at least ~200 ka. At shorter timescales (i.e. decadal), our results are supported by regional geodetic studies which show no relative right-lateral displacement of stations that lie on opposite sides of the Karakoram fault system in the southeast Pamir (Fig. 1C) (Ischuk et al., 2013; Wang et al., 2001; Zhang et al., 2004). Further, recent detailed work on the seismicity of the Pamir suggests the eastern portion of the Pamir are experiencing little internal deformation (Schurr et al., 2014). One complication is the observed seismicity along the dextral Aksu–Murghab fault zone in the southeast Pamir (Strecker et al., 1995), where two earthquakes yielded strongly oblique dextral-normal focal mechanisms (Schurr et al., 2014). However, the strong extensional component of the focal mechanisms are opposite what would be expected for a left bend in the dextral Karakoram fault, and we interpret them to be related to westward extensional collapse of the Pamir (i.e. Schurr et al., 2014).

5.2. Relationship between the Karakoram and Kongur Shan fault systems

Chevalier et al. (2011) determined a dextral slip rate of 4.5 ± 0.2 mm/yr along the east–west striking Muji fault at the northern

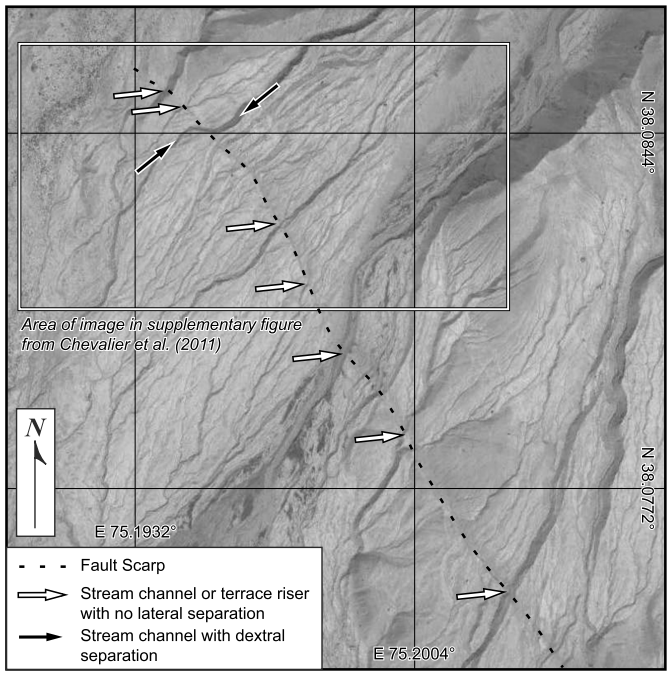

Fig. 6. Google Earth satellite image of a fault scarp along the Kongur Shan normal fault south of Muztagh Ata showing an expanded view of the fault scarp discussed in Chevalier et al. (2011). While several drainages show right-lateral separation across the fault scarp, the majority of stream channels and terrace risers which cross the fault scarp have no lateral deflection showing there is no dextral shear along the Kongur Shan normal fault.

end of the Kongur Shan fault system (Fig. 1A). The authors interpreted the Muji fault (and entire Kongur Shan fault system) to be the northward extension of the Karakoram fault, and suggested that their results revealed a roughly consistent slip rate along the entire 1200 km trace of the Karakoram fault. While our results showing that the northern end of the Karakoram fault has not accommodated detectable slip in the past 200 ka preclude this interpretation, it is important to address several other lines of evidence that show the two fault systems are neither directly connected nor kinematically linked.

Chevalier et al. (2011) interpreted a stream channel with dextral deflection across a recent fault scarp located immediately south of the Muztagh Ata massif as evidence for a dextral component of slip along the north–south striking portions of the Kongur Shan fault system. However, satellite imagery available on Google Earth shows numerous adjacent stream channels and terrace risers along the depicted fault segment with no lateral separation (Fig. 6). Thus the dextrally deflected stream channel of Chevalier et al. (2011) is unrepresentative of stream channels which cross the Kongur Shan fault system, consistent with the lack of laterally offset geomorphic features along the entire 150 km long Kongur Shan normal fault and 50 km long Tashkorgan fault (cf. Li, 2013; Robinson et al., 2004). Further, previous geologic mapping in the Tashkorgan valley shows that faults and recent fault scarps related to the Kongur Shan fault system do not intersect the northern end of the Karakoram fault (Robinson, 2009a; Robinson et al., 2007), precluding a kinematic link between the two structures. Finally, regional geodetic studies show no obvious step (i.e. shear associated with a fault) in the northward velocity gradient across the eastern Pamir salient from the Central Pamir to the Tarim basin (Ischuk et al., 2013; Zubovich et al., 2010), inconsistent with the interpretation of right-lateral displacement on the Kongur Shan normal fault. One aspect to note is that the slip rate on the east–west striking Muji fault determined by Chevalier et al. (2011) is equal to the Late Miocene to recent extension rate across the Kongur Shan normal fault (~5 mm/yr; Robinson et al., 2010, 2004), as well as the geodetic change in east–west velocity across the fault (5–8 mm/yr, Zubovich et al., 2010), consistent with the previous interpretation that the Muji fault is a strike-slip segment within an overall east–west extensional fault system.

6. Broader tectonic implications

Our results showing no late Quaternary slip on the northern Karakoram fault require dramatic along-strike variations in late Quaternary slip rate along the Karakoram fault from ~4–12 mm/yr along the southern fault segment (Brown et al., 2002, 2005; Chevalier et al., 2005, 2012), to no motion at its northern end. These results are consistent with regional InSAR analysis which shows the slip rate on the Karakoram fault falling below the limit of detection north of the Bangong transpressional zone (Wang and Wright, 2012), as well as a lack of observed neotectonic activity along the Nubra valley north of the Bangong transpressional zone (Brown et al., 2002). While similar gradients in slip rate have been documented on other strike slip faults in the Tibetan orogen (i.e. the eastern Kunlun fault, Kirby et al., 2007), these are generally near the tips of faults where both slip rate and finite strain might be expected to decrease, in contrast to the Karakoram fault where the inactive northern segment fault has greater cumulative displacement than the southern segment. We argue that cessation of slip on the northern Karakoram is due to regional kinematic reorganization, with slip formerly accommodated on the northern Karakoram fault now being taken up by the Pliocene to Recent left-slip Longmu Co-Guoza Co fault system of western Tibet (Raterman et al., 2007; Robinson, 2009a). This hypothesis predicts that the Longmu Co-Guoza Co fault system should have a slip rate similar to the southern Karakoram fault (~5–10 mm/yr), broadly consistent with regional InSAR results which indicate ~4 mm/yr of left lateral motion on structures associated with the Longmu Co-Guoza Co fault system (Wang and Wright, 2012). One possible driver for this reorganization is the proposed Pliocene decrease or cessation of slip along the eastern margin of the Pamir (Sobel et al., 2011) which would have decreased the northward velocity of the Pamir relative to Tibet and terminated slip the northern Karakoram fault. Continued slip along the southern Karakoram fault would have been accommodated by initiation of the Longmu Co-Guoza Co fault system as part of the Late Miocene to present conjugate strike-slip faulting in the Tibetan plateau accommodating pure-shear stretching of the Tibetan crust (Taylor et al., 2003). An alternative possibility is that dynamic interactions between the Karakoram fault and the subducting Indian plate may inhibit seismic loading on the northern portion of the fault (Houlié and Phillips, 2013). However, whether this would be effective on the order of hundreds of thousands of years is unclear.

More broadly, our results show that the northern Karakoram fault does not currently form a discrete kinematic boundary within the Himalayan–Tibetan orogen between the Pamir–Karakoram region to the west and the Tibetan Plateau to the east, as assumed in many kinematic and geodynamic models (Avouac and Tapponnier, 1993; He and Chéry, 2008; Liu and Bird, 2008; Loveless and Meade, 2011; Meade, 2007; Peltzer and Saucier, 1996). Instead, the dynamics of the two regions may be partially coupled, or more likely decoupled over a broad region of diffuse deformation, a feature that future kinematic and mechanical models of recent to active deformation in the Tibetan orogen will need to take into consideration. Further, our results suggest that the role of the Karakoram fault may have dramatically changed during its evolution, from initially accommodating differential northward displacement of crust between the Pamir–Karakoram region and the Tibetan Plateau, to accommodating arc-parallel extension of the Himalayan arc and/or

pure-shear deformation of Tibetan crust (Kundu et al., 2014; Murphy et al., 2010, 2014; Styron et al., 2011).

Finally, the lack of late Quaternary activity on the northern Karakoram fault system indicates that even long (i.e. >500 km) strike-slip faults that develop within orogenic belts may be inherently unstable features if not located along major crustal/lithospheric boundaries (such as the Altyn Tagh fault, Wittlinger et al., 1998; Zhao et al., 2006). If so, it follows that slip rates for intra-orogenic strike-slip faults, determined on decadal to millennial timescales should not be extrapolated over much longer timescales (10^6–10^7 years) without due caution (cf. Taylor and Peltzer, 2006). Thus, while rigid block models are suitable to describe the kinematics of the upper crust at decadal to millennial scales (e.g. Loveless and Meade, 2011; Meade, 2007; Thatcher, 2007), the boundaries of these blocks may not remain constant over longer intervals. This would be consistent with general models of continental deformation involving relatively weak crust with distributed deformation over geologic timescales (e.g. England and Houseman, 1988; Houseman and England, 1996).

7. Conclusions

Our field observations, integrated with new geochronologic data and previously published ages, provide new information on the late Quaternary slip history of the Karakoram fault. At the Pisiling site, we document an undeformed strath terrace with overlying gravels that extends across the main strand of the Karakoram fault. Secondary carbonate rims on gravels overlying a correlative terrace yield a U-series age of 198 ± 5 ka, which provides a robust minimum age of terrace formation. At the Mazha'er site, the secondary Achiehkopai fault strand is overlain by undisturbed Hangdi glacial stage (24 ± 6 ka, Owen et al., 2012) deposits and Dabudar glacial stage (likely >200 ka, Owen et al., 2012) deposits lacking observable lateral displacement. Together, our results show the northern end of the Karakoram fault has not accommodated any detectable slip since at least at least 24 ± 6 ka, and most likely since ~ 200 ka or more.

Our results confirm previous interpretations that the Kongur Shan extensional system along the eastern margin of the Pamir evolved independently from, and does not represent a continuation of, the Karakoram fault. Further, our results provide evidence that even long (>500 km) strike-slip faults within orogenic belts may be inherently transient features, consistent with models of continental collision zones involving relatively weak crust and distributed deformation.

Acknowledgements

We thank two anonymous reviewers for comments on a previous version of this paper, and Dr. Ramon Arrowsmith and an anonymous reviewer whose comments and suggestions improved the clarity and presentation of the ideas in this paper. This project was supported by a grant from the Tectonics program at NSF (EAR-0911598) to A.C.R. and L.A.O., a Grants to Enhance and Advance Research (GEAR) grant (IO98426) from the University of Houston to A.C.R., a grant from State Key Laboratory of Earthquake Dynamics of China (LED2010A04) and the International Science and Technology Cooperation Program of China (2008DFA20860) to J.C., Z.Y., and W.L. An NSF Instrumentation and Facilities Grant, NSF EAR1153689, provides support to PRIME Lab.

Appendix A. Supplementary material

Supplementary material related to this article can be found online at http://dx.doi.org/10.1016/j.epsl.2014.11.011.

References

Armijo, R., Tapponnier, P., Tonglin, H., 1989. Late Cenozoic right-lateral strike-slip faulting in southern Tibet. J. Geophys. Res. 94, 2787–2838.

Avouac, J.-P., Tapponnier, P., 1993. Kinematic model of active deformation in central Asia. Geophys. Res. Lett. 20, 895–898.

Banerjee, P., Burgmann, R., 2002. Convergence across the northwest Himalaya from GPS measurements. Geophys. Res. Lett. 29, 1652. http://dx.doi.org/10.1029/2002GL015184.

Brown, E.T., Bendick, R., Bourles, D.L., Gaur, V., Molnar, P., Raisbeck, G.M., Yiou, F., 2002. Slip rates of the Karakorum fault, Ladakh, India, determined using cosmic ray exposure dating of debris flows and moraines. J. Geophys. Res. 107, B9. http://dx.doi.org/10.1029/2000JB000100.

Brown, E.T., Molnar, P., Bourlés, D.L., 2005. Comment on "Slip-Rate Measurements on the Karakorum Fault May Imply Secular Variations in Fault Motion". Science 309, 1326b.

Cheng, H., Lawrence Edwards, R., Shen, C.-C., Polyak, V.J., Asmerom, Y., Woodhead, J., Hellstrom, J., Wang, Y., Kong, X., Spötl, C., Wang, X., Calvin Alexander Jr., E., 2013. Improvements in ^{230}Th dating, ^{230}Th and ^{234}U half-life values, and U–Th isotopic measurements by multi-collector inductively coupled plasma mass spectrometry. Earth Planet. Sci. Lett. 371–372, 82–91.

Chevalier, M.-L., Li, H., Pan, J., Pei, J., Wu, F., Xu, W., Sun, Z., Liu, D., 2011. Fast slip-rate along the northern end of the Karakorum fault system, western Tibet. Geophys. Res. Lett. 38, 7.

Chevalier, M.-L., Ryerson, F.J., Tapponnier, P., Finkel, R.C., Van Der Woerd, J., Haibing, L., Qing, L., 2005. Slip-rate measurements on the Karakorum fault may imply secular variations in fault motion. Science 307, 411–414.

Chevalier, M.-L., Tapponnier, P., Van Der Woerd, J., Ryerson, F.J., Finkel, R.C., Li, H., 2012. Spatially constant slip rate along the southern segment of the Karakorum fault since 200 ka. Tectonophysics 530–531, 152–179.

England, P.C., Houseman, G.A., 1988. The mechanics of the Tibetan Plateau. Philos. Trans. R. Soc. Lond. A 326, 301–319.

He, J., Chéry, J., 2008. Slip rates of the Altyn Tagh, Kunlun and Karakorum faults (Tibet) from 3D mechanical modeling. Earth Planet. Sci. Lett. 274, 50–58.

Holden, N.E., 1989. Total and spontaneous fission half-lives for uranium, plutonium, americium and curium nuclides. Pure Appl. Chem. 61, 1483–1504.

Houlié, N., Phillips, R.J., 2013. Quaternary rupture behavior of the Karakoram Fault and its relation to the dynamics of the continental lithosphere, NW Himalaya–western Tibet. Tectonophysics 599, 1–7.

Houseman, G., England, P., 1996. A lithospheric-thickening model for the Indo-Asian collision. In: Yin, A., Harrison, T.M. (Eds.), The Tectonic Evolution of Asia. Cambridge University Press, New York, pp. 3–17.

Ischuk, A., Bendick, R., Rybin, A., Molnar, P., Khan, S.F., Kuzikov, S., Mohadjer, S., Saydullaev, U., Ilyasova, Z., Schelochkov, G., Zubovich, A.V., 2013. Kinematics of the Pamir and Hindu Kush regions from GPS geodesy. J. Geophys. Res. 118, 9.

Jaffey, A.H., Flynn, K.F., Glendenin, L.E., Bentley, W.C., Essling, A.M., 1971. Precision measurement of half-lives and specific activities of ^{235}U and ^{238}U. Phys. Rev. C, Nucl. Phys. 4, 1889–1906.

Kirby, E., Harkins, N., Wang, E., Fan, C., Burbank, D., 2007. Slip rate gradients along the eastern Kunlun fault. Tectonics 26, 16.

Kundu, B., Yadav, R.K., Bali, B.S., Chowdhury, S., Gahalaut, V.K., 2014. Oblique convergence and slip partitioning in the NW Himalaya: implications from GPS measurements. Tectonics. http://dx.doi.org/10.1002/2014TC003633.

Lacassin, R., Valli, F., Arnaud, N., Leloup, P.H., Papuette, J.L., Haibing, L., Tapponnier, P., Chevalier, M.-L., Guillot, S., Mahéo, G., Zhiqin, X., 2004. Large-scale geometry, offset and kinematic evolution of the Karakorum fault, Tibet. Earth Planet. Sci. Lett. 219, 255–269.

Li, W., 2013. Active tectonics and strong earthquakes in Tashkurgan Valley, Northeast Pamir, China. PhD thesis. China Earthquake Administration, Beijing.

Liu, Z., Bird, P., 2008. Kinematic modelling of neotectonics in the Persia–Tibet–Burma orogen. Geophys. J. Int. 172, 779–797.

Loveless, J.P., Meade, B.J., 2011. Partitioning of localized and diffuse deformation in the Tibetan Plateau from joint inversions of geologic and geodetic observations. Earth Planet. Sci. Lett. 303, 11–24.

Ludwig, K.R., 2003. Using Isoplot/Ex, Version 2.01: A Geochronological Toolkit for Microsoft Excel. Berkeley Geochronology Center, Berkeley, California. 47 pp.

Meade, B.J., 2007. Present-day kinematics at the India–Asia collision zone. Geology 35, 81–84.

Molnar, P., Tapponnier, P., 1978. Active tectonics of Tibet. J. Geophys. Res. 83, 5361–5375.

Murphy, M.A., Sanchez, V., Taylor, M.H., 2010. Syncollisional extension along the India–Asia suture zone, south-central Tibet: implications for crustal deformation of Tibet. Earth Planet. Sci. Lett. 290, 233–243.

Murphy, M.A., Taylor, M.H., Gosse, J., Silver, C.R.P., Whipp, D.M., Beaumont, C., 2014. Limit of strain partitioning in the Himalaya marked by large earthquakes in western Nepal. Nat. Geosci. 7, 38–42.

Murphy, M.A., Yin, A., Kapp, P., Harrison, T.M., Ling, D., Jinghui, G., 2000. Southward propagation of the Karakoram fault system, southwest Tibet: timing and magnitude of slip. Geology 28, 451–454.

Owen, L.A., Chen, J., Hedrick, K.A., Caffee, M.W., Robinson, A.C., Schoenbohm, L.M., Yuan, Z., Li, W., Imrecke, D.B., Liu, J., 2012. Quaternary glaciation of the Tashkurgan Valley, Southeast Pamir. Quat. Sci. Rev. 47, 56–72.

Peltzer, G., Saucier, F., 1996. Present-day kinematics of Asia derived from geologic fault rates. J. Geophys. Res. 101, 27943–27956.

Peltzer, G., Tapponnier, P., 1988. Formation and evolution of strike-slip faults, rifts, and basins during the India–Asia collision: an experimental approach. J. Geophys. Res. 93, 15085–15117.

Phillips, R.J., Parrish, R.R., Searle, M.P., 2004. Age constraints on ductile deformation and long-term slip rates along the Karakoram fault zone, Ladakh. Earth Planet. Sci. Lett. 226, 305–319.

Raterman, N.S., Cowgill, E., Lin, D., 2007. Variable structural style along the Karakoram fault explained using triple-junction analysis of intersecting faults. Geosphere 3, 71–85.

Replumaz, A., Tapponnier, P., 2003. Reconstruction of the deformed collision zone between India and Asia by backward motion of lithospheric blocks. J. Geophys. Res. 108, 2285. http://dx.doi.org/10.1029/2001JB000661.

Robinson, A.C., 2009a. Evidence against Quaternary slip on the northern Karakorum Fault suggests kinematic reorganization at the western end of the Himalayan–Tibetan orogen. Earth Planet. Sci. Lett. 286, 158–170.

Robinson, A.C., 2009b. Geologic offsets across the northern Karakorum fault: implications for its role and terrane correlations in the western Himalayan–Tibetan orogen. Earth Planet. Sci. Lett. 279, 123–130.

Robinson, A.C., Yin, A., Lovera, O.M., 2010. The role of footwall deformation and denudation in controlling cooling age patterns of detachment systems: an application to the Kongur Shan extensional system in the Eastern Pamir, China. Tectonophysics 496, 28–43.

Robinson, A.C., Yin, A., Manning, C.E., Harrison, T.M., Zhang, S.-H., Wang, X.-F., 2004. Tectonic evolution of the northeastern Pamir: constraints from the northern portion of the Cenozoic Kongur Shan extensional system. Geol. Soc. Am. Bull. 116, 953–974.

Robinson, A.C., Yin, A., Manning, C.E., Harrison, T.M., Zhang, S.-H., Wang, X.-F., 2007. Cenozoic evolution of the eastern Pamir: implications for strain-accommodation mechanisms at the western end of the Himalayan–Tibetan orogen. Geol. Soc. Am. Bull. 119, 882–896.

Schurr, B., Ratschbacher, L., Sippl, C., Gloaguen, R., Yuan, X., Mechie, J., 2014. Seismotectonics of the Pamir. Tectonics 33, 1501–1518.

Searle, M.P., 1996. Geological evidence against large-scale pre-Holocene offsets along the Karakoram Fault: implications for the limited extrusion of the Tibetan Plateau. Tectonics 15, 171–186.

Searle, M.P., Elliott, J.R., Phillips, R.J., Chung, S.-L., 2011. Crustal–lithospheric structure and continental extrusion of Tibet. J. Geol. Soc. 168, 633–672.

Searle, M.P., Weinberg, R.F., Dunlap, W.J., 1998. Transpressional tectonics along the Karakoram fault zone, northern Ladakh: constraints on Tibetan extrusion. In: Holdsworth, R.E., Strachan, R.A., Dewey, J.F. (Eds.), Continental Transpressional and Transtensional Tectonics. Geological Society of London Special Publication, London, pp. 307–326.

Sobel, E., Schoenbohm, L.M., Chen, J., Thiede, R., Stockli, D.F., Sudo, M., Strecker, M.R., 2011. Late Miocene–Pliocene deceleration of dextral slip between Pamir and Tarim: implications for Pamir orogenesis. Earth Planet. Sci. Lett. 304, 369–378.

Strecker, M.R., Frisch, W., Hamburger, M.W., Ratschbacher, L., Semiletkin, S., Zamoruyev, A., Sturchio, N., 1995. Quaternary deformation in the Eastern Pamirs, Tadzhikistan and Kyrgyzstan. Tectonics 14, 1061–1079.

Styron, R.H., Taylor, M.H., Murphy, M.A., 2011. Oblique convergence, arc-parallel extension, and the role of strike-slip faulting in the High Himalaya. Geosphere 7, 582–596.

Tapponnier, P., Peltzer, G., Le Dain, A.Y., Armijo, R., Cobbold, P., 1982. Propagating extrusion tectonics in Asia: new insights from simple experiments with plasticine. Geology 10, 611–616.

Taylor, M., Peltzer, G., 2006. Current slip rates on conjugate strike-slip faults in central Tibet using synthetic aperture radar interferometry. J. Geophys. Res. 111. http://dx.doi.org/10.1029/2005JB004014.

Taylor, M., Yin, A., 2009. Active structures of the Himalayan–Tibetan orogen and their relationships to earthquake distribution, contemporary strain field, and Cenozoic volcanism. Geosphere 5, 199–214.

Taylor, M., Yin, A., Ryerson, F.J., Kapp, P., Ding, L., 2003. Conjugate strike-slip faulting along the Bangong–Nujiang suture zone accommodates coeval east–west extension and north–south shortening in the interior of the Tibetan Plateau. Tectonics 22. http://dx.doi.org/10.1029/2002TC001361. 18 pp.

Thatcher, W., 2007. Microplate model for the present-day deformation of Tibet. J. Geophys. Res. 112. http://dx.doi.org/10.1029/2005JB004244.

Valli, F., Arnaud, N., Leloup, P.H., Sobel, E.R., Mahéo, G., Lacassin, R., Guillot, S., Li, H., Tapponnier, P., Xu, Z., 2007. Twenty million years of continuous deformation along the Karakorum fault, western Tibet: a thermochronological analysis. Tectonics 26.

Wang, H., Wright, T.J., 2012. Satellite geodetic imaging reveals internal deformation of western Tibet. Geophys. Res. Lett. 39.

Wang, Q., Zhang, P.-Z., Freymueller, J., Bilham, R., Larson, K., Lai, X.a., You, X., Niu, Z., Wu, J., Li, Y., Liu, J., Yang, Z., Chen, Q., 2001. Present-day crustal deformation in China constrained by global positioning system measurements. Science 294, 274–577.

Wang, S., Wang, C., Phillips, R.J., Murphy, M.A., Fang, X., Yue, Y., 2012. Displacement along the Karakoram fault, NW Himalaya, estimated from LA-ICP-MS U–Pb dating of offset geologic markers. Earth Planet. Sci. Lett. 337–338, 156–163.

Wittlinger, G., Tapponnier, P., Poupinet, G., Mei, J., Danian, S., Herquel, G., Masson, F., 1998. Tomographic evidence for localized lithospheric shear along the Altyn Tagh Fault. Science 282, 74.

Wright, T.J., Parsons, B., England, P.C., Fielding, E.J., 2004. InSAR observations of low slip rates on the major faults of Western Tibet. Science 305, 236–239.

Zhang, P.-Z., Shen, Z., Wang, M., Gan, W., Burgmann, R., Molnar, P., Wang, Q., Niu, Z., Sun, J., Wu, J., Hanrong, S., Xinzhao, Y., 2004. Continuous deformation of the Tibetan Plateau from global positioning system data. Geology 32, 809–812.

Zhao, J., Mooney, W.D., Zhang, X., Li, Z., Jin, Z., Okaya, N., 2006. Crustal structure across the Altyn Tagh Range at the northern margin of the Tibetan plateau and tectonic implications. Earth Planet. Sci. Lett. 241, 804–814.

Zubovich, A.V., Wang, X.-q., Scherba, Y.G., Schelochkov, G.G., Reilinger, R., Reigber, C., Mosienko, O.I., Molnar, P., Michajljow, W., Makarov, V., Li, J., Kuzikov, S.I., Herring, T.A., Hamburger, M.W., Hager, B.H., Dang, Y.-m., Bragin, V.D., Beisenbaev, R.T., 2010. GPS velocity field for the Tien Shan and surrounding regions. Tectonics 29, 23.